JACS
JOURNAL OF THE AMERICAN CHEMICAL SOCIETY
pubs.acs.org/JACS
Article

A *De Novo* CO_2 Reductase Featuring a Cysteine-Ligated Cobalt Porphyrin Cofactor

Emily J. Radley,[†] Alessia C. Andrews,[†] Indrek Kalvet, Yunling Deng, Elizabeth L. Bell, Colin W. Levy, Mary Ortmayer, Derren J. Heyes, Clare F. Megarity, Reyes Núñez-Franco, Amy E. Hutton, Yi Lu, David Baker,* and Anthony P. Green*

Cite This: https://doi.org/10.1021/jacs.6c07615
Read Online

ABSTRACT: Modern protein design methods based on deep learning allow generation of customized protein scaffolds with diverse geometries and functionalities. Here we capitalize on these recent advances to develop hyper-thermostable *de novo* CO_2 reductases featuring a cobalt porphyrin IX (CoPPIX) cofactor. CoPPIX-containing enzymes were assembled *in vivo* through media supplementation with cobalt salts and assessed for photocatalytic CO_2 reductase activity. We identified two cysteine-ligated designs that exhibit high activity (>1000 turnovers at rates of up to 25 min^{-1}) while suppressing competing hydrogen evolution pathways. A 2.1 Å crystal structure shows close agreement to the design model with the Co−Cys bond programmed as intended. This study showcases the power of computational protein design in developing artificial enzymes to activate challenging molecules such as CO_2.

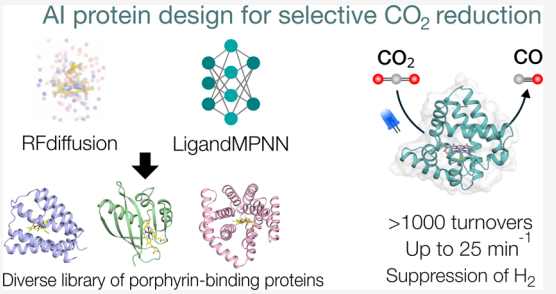

INTRODUCTION

Rising CO_2 levels in the atmosphere are a major driver of global warming. To facilitate the transition to net-zero, new catalytic technologies to transform CO_2 into platform chemicals are needed. In this regard, a variety of homogeneous and heterogeneous catalysts have been developed for reducing CO_2 to CO and other C_1 products.[1−10] Although these systems can offer high catalytic rates, they commonly suffer from poor stability and/or compromised selectivity as they are unable to discriminate between competing CO_2 and proton reduction pathways.[11,12] In contrast, enzymes have evolved in nature to transform CO_2 with remarkable efficiency and selectivity.[13−21] Unfortunately, these natural systems are often only marginally stable and can be challenging to produce and characterize.[22−24] As a result, the structural features that underpin activation and transformation of CO_2 in native enzymes are still not fully understood. One approach to overcome these limitations is to develop artificial metalloenzymes within small stable protein scaffolds that are amenable to engineering.[25−27] This approach can provide new insights into the factors governing selective CO_2 conversion and lead to the development of biocatalysts with improved properties. As an example, we have recently developed artificial CO_2 reductases by reconstituting myoglobin variants with a non-native cobalt protoporphyrin IX (CoPPIX) cofactor.[28] These artificial enzymes mediate photocatalytic conversion of CO_2 to CO with enhanced activity and selectivity (CO formation vs H_2 production) compared to small synthetic Co-porphyrin cofactors.[27−31]

In principle, these myoglobin-based systems could serve as starting templates for evolutionary optimization to deliver highly active, selective, and specialized CO_2 reductases. However, establishing suitable high-throughput directed evolution pipelines for this class of transformation presents considerable challenges linked to difficulties in performing high-throughputquantitative analysis of gas phase products. In light of these constraints, we instead turned to modern protein design methods in an effort to generate artificial metalloenzymes with improved properties. Our laboratories have recently developed hyper-stable peroxidases and carbene transferases featuring a histidine-ligated Fe-porphyrin in a *de novo* α-helical solenoid repeat scaffold.[32] These studies provided insights into the factors leading to high-affinity porphyrin binding within *de novo* proteins. Armed with this knowledge, and with powerful deep learning-based methods now available for generating protein ligand complexes (e.g., RFdiffusion All-Atom[33] and LigandMPNN[34]), we have the opportunity to create porphyrin-binding proteins with diverse active site geometries, cofactor coordination environments, and topologies that extend far beyond those found in nature. We set out to use these methods to generate a family of

Received: April 13, 2026
Revised: June 10, 2026
Accepted: June 12, 2026

https://doi.org/10.1021/jacs.6c07615
J. Am. Chem. Soc. XXXX, XXX, XXX−XXX

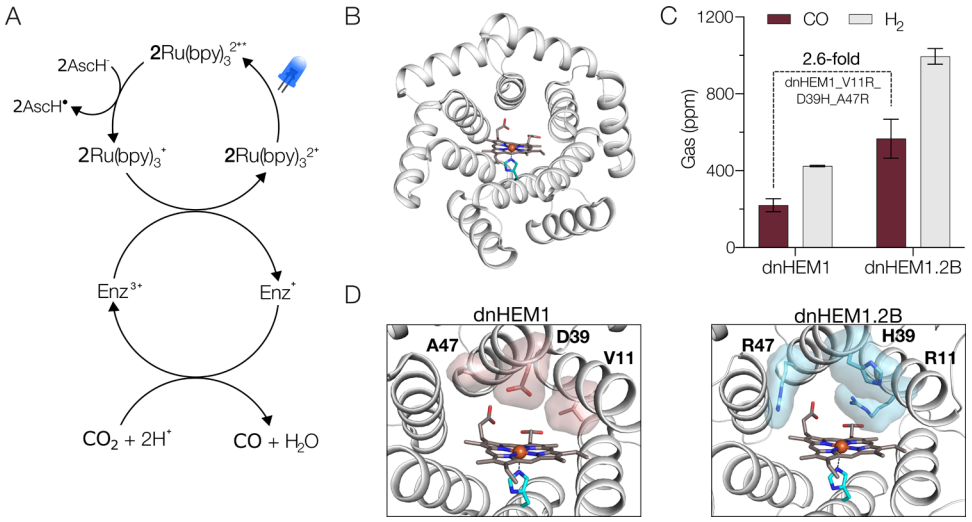

Figure 1. Development of first-generation *de novo* CO_2 reductases. (A) Simplified schematic of the photocatalytic cycle for enzymatic reduction of CO_2 to CO using $[Ru(bpy)_3]^{2+}$ as a photosensitizer. AscH = sodium L-ascorbate. (B) Crystal structure of dnHEM1 (PDB ID 8C3W) highlighting the heme cofactor (atom-colored sticks with dark gray carbons) and the axial histidine (atom-colored sticks with blue teal carbons). (C) Bar chart comparing the CO_2 reductase activity of CoPPIX-loaded dnHEM1 and dnHEM1.2B monitoring CO (plum) and H_2 (gray) production. Biotransformations were performed using 0.3 μM holo-enzyme, 100 mM sodium L-ascorbate, 100 mM sodium bicarbonate, 100 μM $[Ru(bpy)_3]^{2+}$ in 500 mM potassium phosphate buffer (pH 7.0), and irradiation under blue light (475 nm) for 30 min. Error bars represent the range of values from measurements made in duplicate. (D) Active sites of dnHEM1 (PDB ID 8C3W) and dnHEM1.2B (design model) showing axial histidine (atom-colored sticks with blue teal carbons) and heme cofactor (atom-colored sticks with dark gray carbons), with the mutations between dnHEM1 and dnHEM1.2B highlighted in pink and blue, respectively.

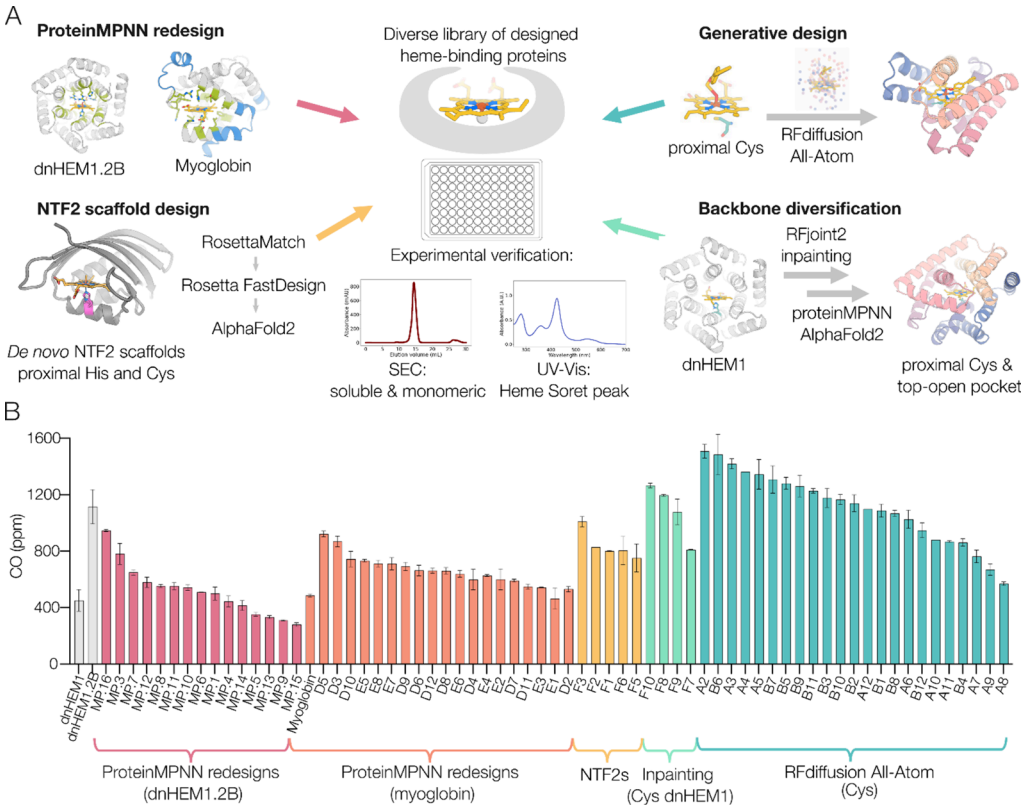

Figure 2. Design and screening of *de novo* CO_2 reductases. (A) Schematic of the heme-binding protein design pipelines using multiple *de novo* computational design methods. (B) Bar chart displaying amount of CO (ppm) produced by the panel of CoPPIX-loaded *de novo* designs compared to dnHEM1 and dnHEM1.2B (gray). The panel includes ProteinMPNN redesigns of dnHEM1.2B (pink), ProteinMPNN redesigns of myoglobin (orange), NTF2 scaffold-based designs (yellow), inpainting of Cys-ligated dnHEM1 designs (green), and designs generated by RFdiffusion All-Atom (teal). Biotransformations were performed using enzyme normalized to a λ_{Soret} absorbance of 0.1, 100 mM sodium L-ascorbate, 100 mM sodium bicarbonate, 100 μM $[Ru(bpy)_3]^{2+}$ in 500 mM potassium phosphate buffer (pH 7.0), and irradiation under blue light (475 nm) for 30 min at room temperature. Error bars represent the range of values from measurements made in duplicate.

https://doi.org/10.1021/jacs.6c07615
J. Am. Chem. Soc. XXXX, XXX, XXX−XXX

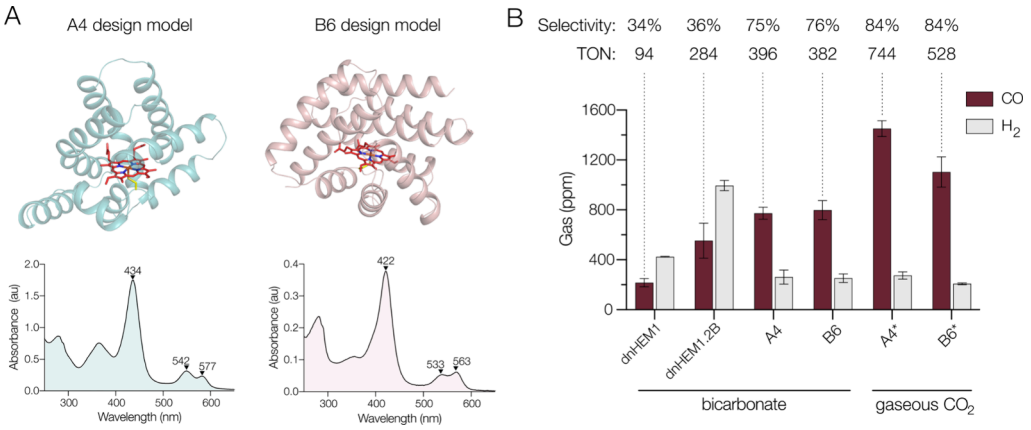

Figure 3. Characterization of designs A4 and B6. (A) AlphaFold2-predicted models of A4 (teal) and B6 (pink) showing the axially ligated heme as red atom-colored sticks and UV−vis spectra of A4 (teal) and B6 (pink). (B) Bar chart comparing the CO_2 reductase (plum) and hydrogen evolution (gray) activities of dnHEM1, dnHEM1.2B, A4, and B6. Biotransformations were performed using 0.3 μM holo-enzyme, 100 mM sodium L-ascorbate, 100 μM $[Ru(bpy)_3]^{2+}$ in 500 mM potassium phosphate buffer (pH 7.0) with either 100 mM sodium bicarbonate or gaseous CO_2 as the CO_2 source, and irradiation under blue light (475 nm) for 30 min. Error bars represent the range of values from measurements made in duplicate.

structurally diverse CoPPIX-binding proteins and investigate their CO_2 reductase activities.

RESULTS AND DISCUSSION

As a starting template for engineering *de novo* CO_2 reductases we selected dnHEM1, a hyper-stable α-helical solenoid that employs an axial histidine ligand to coordinate iron protoporphyrin IX (FePPIX) with high affinity (Figure 1B).[32] To replace the FePPIX with CoPPIX, we adapted a previously reported strategy for *in vivo* cofactor biogenesis and incorporation[35] that obviates the need for costly *in vitro* cofactor replacement steps.[36,37] The UV−vis spectrum of purified CoPPIX-loaded dnHEM1 exhibits a diagnostic Soret feature at 422 nm, shifted from 402 nm as observed with FePPIX-loaded dnHEM1, consistent with successful incorporation of CoPPIX[35] (Figure S1).

We next evaluated the photocatalytic activity of dnHEM1 for CO_2 reduction under anaerobic conditions, employing $[Ru(bpy)_3]^{2+}$ as a photosensitizer, sodium bicarbonate as a CO_2 source and sodium L-ascorbate as a sacrificial reductant under blue light irradiation (475 nm) for 30 min (Figure 1A). Samples of the reaction headspace following photoirradiation were analyzed by gas chromatography (GC). Under these conditions, dnHEM1 produces 220 ppm of CO (94 turnovers in 30 min) alongside 424 ppm of H_2. In an attempt to further improve activity, we sampled an in-house panel of dnHEM1 variants that have previously been engineered to enhance heme peroxidase or carbene transferase activity.[32] From these assays, we identified dnHEM1.2B (dnHEM1_V11R_D39H_A47R, Figure 1D) that displays a 2.6-fold improvement in CO_2 reductase activity (241 turnovers in 30 min), albeit with similar selectivity to that observed with dnHEM1 (Figure 1C).

Having developed a first-generation *de novo* CO_2 reductase, we next sought to explore a broader range of protein sequences and scaffolds to identify more potent and selective enzymes. We used multiple design strategies to generate heme-binding proteins featuring either cysteine or histidine as an axial ligand (Figure 2A). Sequence diverse artificial homologues of myoglobin[38] and dnHEM1.2B were generated using a combination of ProteinMPNN and RFjoint2 inpainting.[39] These approaches were extended to generate heme-binders in *de novo* NTF2 scaffolds.[40−42] To explore a wider variety of protein topologies and active site configurations, we turned to generative AI based protein design methods. We have previously generated and characterized tens of *de novo* Cys-ligated heme-binding proteins based on RFdiffusion All-Atom protein backbone generation.[33] To expand this set, we started new design trajectories from a minimal active site model consisting of an axially ligated heme with a spatial placeholder in the distal site. The amino acid sequences were then optimized by iterative application of ProteinMPNN,[43] LigandMPNN,[34] Rosetta FastRelax,[44] and AlphaFold2.[45] Designed proteins were evaluated for AlphaFold2 confidence and accuracy, as well as for Rosetta metrics describing the protein−ligand interface quality. Synthetic DNA fragments encoding the designed proteins from each of the design pipelines were assembled into the pET29b plasmid for expression in *Escherichia coli*.[46,47] Following evaluation of the soluble expression levels and heme-binding properties of these designs, we selected a total of 69 well-performing sequences from 26 unique protein folds for CoPPIX incorporation and activity studies (Table S1).

The panel of designs was expressed in *E. coli* using the protocol described above for *in vivo* CoPPIX incorporation. Of the 69 sequences selected, 67 were expressed in soluble form and readily purified via nickel affinity chromatography; 63 of these designs displayed UV−vis spectral features diagnostic of CoPPIX incorporation (λ_{Soret} values from 420 to 435 nm)[27,35,48−50] (Figures S2−S6). The remaining four designs have more complex UV−vis absorbance profiles (Figure S7), potentially rising from mixed oxidation states and/or partial spin states.[35,51]

The above 67 purified designs were subsequently evaluated for photocatalytic CO_2 reduction activity using the headspace GC assay (Figure 2B). While sequence redesigns of dnHEM1.2B gave several variants with improved CO formation versus dnHEM1, this approach failed to yield any artificial homologues with improved activity compared to dnHEM1.2B. Similarly, redesigns based on myoglobin as a template (PDB ID 3RGK) gave some improvements over the wild-type sequence but again failed to surpass the activity of dnHEM1.2B. Greater success was achieved using inpainting to

https://doi.org/10.1021/jacs.6c07615
J. Am. Chem. Soc. XXXX, XXX, XXX−XXX

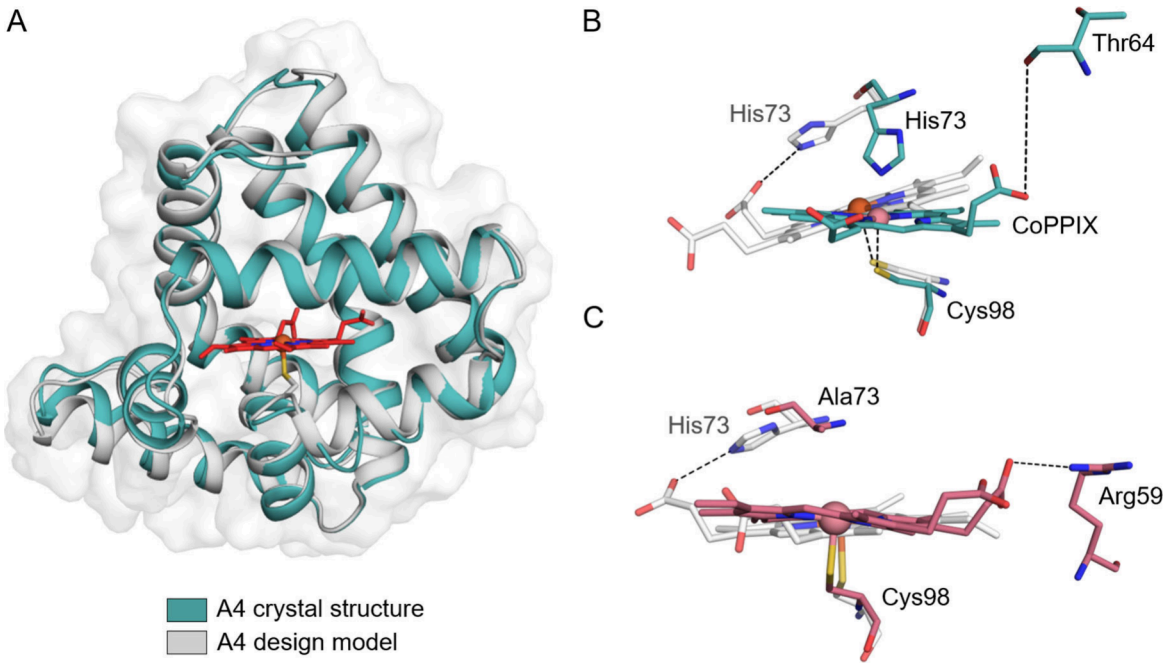

Figure 4. Structural analysis of A4 and A4 H73A. (A) Crystal structure of A4 (teal) (PDB ID 9T8A), showing close agreement to the AlphaFold2 design model (gray). The cysteine-ligated heme of the design model is shown as red atom-colored sticks. (B) Comparison of the active site of A4 (teal atom-colored sticks) and the A4 design model (gray atom-colored sticks) highlighting the differences in positioning of His73 and the porphyrin cofactor. In the design model, His73 forms interactions with the propionate group of the cofactor, whereas in the crystal structure it coordinates the CoPPIX cofactor to form a hexa-coordinated complex. (C) Comparison of the active site of A4 H73A (PDB ID 9T8B) (pink atom-colored sticks) and the A4 design model (gray atom-colored sticks). In the A4 H73A structure the CoPPIX cofactor is pentacoordinated as required for catalysis, with the porphyrin plane and positioning of the axial cysteine now more closely resembling the design model.

introduce an axial cysteine ligand into dnHEM1 which gave small improvements over dnHEM1.2B. Evaluation of designs generated using RFdiffusion All-Atom incorporating a cysteine ligand led to the identification of 11 structurally diverse designs that displayed activity greater than or equal to dnHEM1.2B. Of the top performing designs, A2 and A3 share a common fold but had a propensity to precipitate during purification. We therefore selected A4 and B6, which display similarly high activity, for further characterization. We note that these designs bear no resemblance to any protein observed in nature, as indicated by template modeling (TM) scores of 0.54 and 0.56, respectively[52] (Figure S8).

Following production of A4 and B6 under optimized expression conditions, the designs were purified by nickel affinity chromatography followed by size exclusion chromatography (SEC), which allowed separation of holo-proteins from soluble protein aggregates (Figure S9). Both holo-proteins eluted as monomeric species as confirmed by SEC-MALS (Figure S10). UV−vis spectroscopy showed that A4 exhibits a sharp Soret band at 434 nm with Q-band features at 542 and 577 nm, whereas B6 displays a Soret band at 422 nm with Q-band features at 533 and 563 nm (Figure 3A). CoPPIX incorporation was quantified using inductively coupled plasma optical emission spectrometry (ICP-OES) and used to determine Soret extinction coefficients of 104.4 and 97.4 mM^{-1} cm^{-1} for A4 and B6, respectively (Table S2). No iron contamination was detected in any sample by ICP-OES. A4 and B6 are both hyper-thermostable (T_m > 95 °C), showing minimal changes in circular dichroism (CD) spectra from 25−95 °C. Cofactor retention was also preserved at 95 °C, with negligible shifts in Soret intensity or wavelength (Figure S11).

With purified enzymes in hand, we next compared the activity and selectivity of A4, B6, dnHEM1, and dnHEM1.2B. Consistent with the initial panel screening, A4 and B6 exhibited 3.6- and 3.7-fold improvements in CO_2 reduction activity compared to dnHEM1, respectively. These activity gains were accompanied by a marked increase in selectivity for CO_2 reduction over H_2 generation (*ca.* 75% selectivity with A4 and B6 vs *ca.* 35% with dnHEM1 and dnHEM1.2B) (Figure 3B). It is known that photoactivated $[Ru(bpy)_3]^{2+}$ can drive H_2 evolution,[53] and control experiments show that hydrogen production is significantly reduced in the presence of A4 and B6 (Figure S12). These observations suggest that the intrinsic selectivity associated with A4 and B6 is likely substantially higher than 75%. Time-course experiments show that A4 and B6 can achieve TTN_{CO} values of 580 and 620, prior to deactivation (Figure S13). Improvements in reaction rate, selectivity, and total turnovers can be achieved by replacing bicarbonate with gaseous CO_2 as the substrate. Using A4 and B6 as biocatalysts, CO_2 can be converted to CO with >84% selectivity at rates of 25 and 18 min^{-1}, respectively, and >1000 total turnovers were achieved for each prior to enzyme deactivation (Figure 3B, Table S3, and Figure S13).

We next sought to solve structures of A4 and B6 for comparison to the design models. While B6 proved difficult to crystallize, the crystal structure of A4 was determined to a resolution of 2.1 Å (PDB ID 9T8A). This structure closely agrees with the AlphaFold2 design model of A4, with a backbone RMSD of 1.05 Å (Figure 4A). The CoPPIX cofactor resides in a solvent-occluded pocket (solvent-accessible surface area of 12 $Å^2$ vs 112 $Å^2$ for dnHEM1; Figure S14) and is ligated through Cys98 as intended. However, His73, designed to interact with one of the CoPPIX propionate groups, instead

https://doi.org/10.1021/jacs.6c07615
J. Am. Chem. Soc. XXXX, XXX, XXX−XXX

occupies the vacant coordination site to generate a hexacoordinated state, which also results in a minor displacement of the porphyrin cofactor relative to the model. The His73 conformer observed in the X-ray structure was occluded in the design model by the surrogate distal site ligand used as a placeholder in the design pipeline (Figure 4B). In the A4 crystal structure, the porphyrin also adopts a rotated geometry relative to the design model, leading to polar interactions between the CoPPIX propionate and Thr64. An AlphaFold3[54] model of A4 with heme agrees with the crystal structure both regarding the orientation of the porphyrin, as well as the His73 conformer (Figure S15).

To understand the functional significance of Cys98 and His73, we independently mutated these residues to alanine. Substitution of Cys98 led to a decrease in CoPPIX-binding, activity and selectivity, demonstrating that the programmed cysteine ligand plays a key role in CoPPIX-dependent CO_2 reduction (Figures S16 and S17). In contrast, the impact of the H73A mutation was found to be negligible. A 1.8 Å resolution structure of A4 H73A (PDB ID 9T8B) shows that while the porphyrin still adopts the rotated geometry observed in A4, its plane and the positioning of the axial Cys98 ligand now more closely resemble that of the design model. In this structure, the CoPPIX cofactor is now pentacoordinated as required for catalysis (Figure 4C).

In summary, this study illustrates how deep learning-based protein design can be used to generate artificial metalloenzymes to transform difficult-to-activate molecules such as CO_2. By sampling designs with diverse topologies, active-site architectures and cofactor coordination environments, we identified several enzymes featuring a Cys-ligated CoPPIX cofactor that display enhanced CO_2 reductase activity while minimizing competing off-pathway H_2 evolution processes. In general, we found that designs featuring an axial cysteine ligand gave an improved activity/selectivity compared with those featuring a less electron-donating histidine. In contrast, the low background activity of free CoPPIX in solution is unaffected by the addition of cysteine or histidine (Figure S12). These combined results suggest that while CO_2 reductase activity and selectivity is sensitive to the identity of the axial ligand, a wider network of active site features and overall protein topology also contribute to CO_2 binding and transformation.

With limited guiding principles to steer active site design, and technically challenging experimental protocols that preclude standard directed evolution methods to optimize enzyme activity, the discoveries outlined in this study would not have been possible without access to a diverse set of protein scaffolds hosting the catalytic CoPPIX cofactor. Moving forward, there are opportunities to extend our enzyme design pipeline to achieve more valuable conversions of CO_2 into C_2 and C_3 platform chemicals that may also be more amenable to high-throughput quantification to underpin directed evolution workflows. In this way, we aim to deliver a new generation of efficient, selective, and stable CO_2-transforming enzymes to help achieve our net-zero goals.

■ ASSOCIATED CONTENT

Data Availability Statement

Accession codes 9T8A and 9T8B contain the coordinates and associated structure factors of A4 and A4 H73A, respectively, that have been deposited in the Protein Data Bank (PDB). Computational models of the designed proteins are available for download at Zenodo under the identifier 10.5281/zenodo.1861569955.[55]

Supporting Information

The Supporting Information is available free of charge at https://pubs.acs.org/doi/10.1021/jacs.6c07615.

Experimental procedures, supplementary data, DNA and protein sequences, primers, and compound characterization (PDF)

■ AUTHOR INFORMATION

Corresponding Authors

Anthony P. Green − *Department of Chemistry, University of Manchester, Manchester Institute of Biotechnology, Manchester M1 7DN, U.K.*; orcid.org/0000-0003-0454-1798; Email: anthony.green@manchester.ac.uk

David Baker − *Institute for Protein Design, University of Washington, Seattle, Washington 98195, United States; Department of Biochemistry and Howard Hughes Medical Institute, University of Washington, Seattle, Washington 98195, United States*; Email: dabaker@uw.edu

Authors

Emily J. Radley − *Department of Chemistry, University of Manchester, Manchester Institute of Biotechnology, Manchester M1 7DN, U.K.*

Alessia C. Andrews − *Department of Chemistry, University of Manchester, Manchester Institute of Biotechnology, Manchester M1 7DN, U.K.*

Indrek Kalvet − *Institute for Protein Design, University of Washington, Seattle, Washington 98195, United States; Department of Biochemistry and Howard Hughes Medical Institute, University of Washington, Seattle, Washington 98195, United States*; orcid.org/0000-0002-6610-2857

Yunling Deng − *Department of Chemistry, University of Texas at Austin, Austin, Texas 78712, United States*; orcid.org/0000-0001-7157-144X

Elizabeth L. Bell − *Department of Chemistry, University of Manchester, Manchester Institute of Biotechnology, Manchester M1 7DN, U.K.*

Colin W. Levy − *Department of Chemistry, University of Manchester, Manchester Institute of Biotechnology, Manchester M1 7DN, U.K.*

Mary Ortmayer − *Department of Chemistry, University of Manchester, Manchester Institute of Biotechnology, Manchester M1 7DN, U.K.*; orcid.org/0000-0002-2521-967X

Derren J. Heyes − *Department of Chemistry, University of Manchester, Manchester Institute of Biotechnology, Manchester M1 7DN, U.K.*; orcid.org/0000-0002-7453-1571

Clare F. Megarity − *Department of Chemistry, University of Manchester, Manchester Institute of Biotechnology, Manchester M1 7DN, U.K.*; orcid.org/0000-0002-0331-916X

Reyes Núñez-Franco − *Institute for Protein Design, University of Washington, Seattle, Washington 98195, United States; Department of Biochemistry and Howard Hughes Medical Institute, University of Washington, Seattle, Washington 98195, United States*

https://doi.org/10.1021/jacs.6c07615
J. Am. Chem. Soc. XXXX, XXX, XXX−XXX

Amy E. Hutton − *Department of Chemistry, University of Manchester, Manchester Institute of Biotechnology, Manchester M1 7DN, U.K.*

Yi Lu − *Department of Chemistry, University of Texas at Austin, Austin, Texas 78712, United States;* orcid.org/0000-0003-1221-6709

Complete contact information is available at: https://pubs.acs.org/10.1021/jacs.6c07615

Author Contributions

†E.J.R. and A.C.A. contributed equally.

Notes

The authors declare no competing financial interest.

■ ACKNOWLEDGMENTS

This work was funded by the Engineering and Physical Sciences Research Council (EPSRC) and bp through the bp International Centre for Advanced Materials (bp-ICAM) for an ICASE to E.J.R. (EP/W522065/1), a Prosperity Partnership funded by EPSRC and bp through the bp-ICAM (Grants ICAM75, ICAM80, and ICAM83) and Johnson Matthey plc to E.J.R. and A.C.A. (EP/V056565/1), and EPSRC to A.P.G. and D.B. (EPSRC Centre-to-Centre Partnership, EP/Z531157/1). We are grateful to the Manchester SYNBIOCHEM Centre (BB/M017702/1), the Future Biomanufacturing Hub (EP/S01778X/1), and the Henry Royce Institute for Advanced Materials (financed through EPSRC Grants EP/R00661X/1, EP/S019367/1, EP/P025021/1, and EP/P025498/1) for access to their facilities. We acknowledge assistance given by Research IT and the use of the Computational Shared Facility at the University of Manchester. We thank J. Tibble-Howlings from the Analytical Services and Instrumentation at the University of Manchester for their expertise and support in ICP-OES measurements. We acknowledge Dr. Holly Birchenough from the Biomols facility at the University of Manchester for providing access to SEC-MALS. The authors thank Diamond Light Source for beamtime on i03 and i04 (proposals MX38021-12 and MX31850-102). We thank the Open Philanthropy Project Improving Protein Design Fund (D.B., I.K.), the Howard Hughes Medical Institute (D.B., I.K.), MCIN/AEI/10.13039/501100011033 (Grants PID2024-160774OB-I00 and PID2021-125946OB-I00 to R.N.-F.), and NERSC for access to the Perlmutter high-performance computing resources (Award BER-ERCAP0022018). We thank Luki Goldschmidt and Kandise VanWormer for maintaining the computational and wet-lab resources at the Institute for Protein Design. We thank Xinting Li for assistance with mass spectrometry experiments at the Institute for Protein Design. We thank Dr. Florence Hardy and Dr. Nathan Ennist for helpful discussions, Dr. Christopher Norn for providing the *de novo*-designed NTF2 scaffolds, and Dr. David Juergens for assistance with RFjoint2 inpainting.

■ ABBREVIATIONS

SEC, size exclusion chromatography; SEC-MALS, size exclusion chromatography−multiangle light scattering; CoPPIX, cobalt protoporphyrin IX; ICP-OES, inductively coupled plasma−optical emission spectroscopy; FePPIX, iron protoporphyrin IX; TTN, total turnover number; *E. coli*, *Escherichia coli*

■ REFERENCES

(1) Chueh, W. C.; Haile, S. M. Ceria as a Thermochemical Reaction Medium for Selectively Generating Syngas or Methane from H_2O and CO_2. *ChemSusChem* **2009**, *2* (8), 735−739.

(2) Yang, Y.; Evans, J.; Rodriguez, J. A.; White, M. G.; Liu, P. Fundamental Studies of Methanol Synthesis from CO_2 Hydrogenation on Cu(111), Cu Clusters, and Cu/ZnO(000). *Phys. Chem. Chem. Phys.* **2010**, *12* (33), 9909−9917.

(3) Deguchi, M.; Yotsuhashi, S.; Yamada, Y.; Ohkawa, K. Photoelectrochemical CO_2 Conversion to Hydrocarbons Using an AlGaN/GaN-Si Tandem Photoelectrode. *Adv. Condens. Matter Phys.* **2015**, *2015* (1), 537860.

(4) Almomani, F.; Bhosale, R.; Khraisheh, M.; Kumar, A.; Tawalbeh, M. Photocatalytic Conversion of CO_2 and H_2O to Useful Fuels by Nanostructured Composite Catalysis. *Appl. Surf. Sci.* **2019**, *483*, 363−372.

(5) Chu, W.-Y.; Culakova, Z.; Wang, B. T.; Goldberg, K. I. Acid-Assisted Hydrogenation of CO_2 to Methanol in a Homogeneous Catalytic Cascade System. *ACS Catal.* **2019**, *9* (10), 9317−9326.

(6) Scharnagl, F. K.; Hertrich, M. F.; Neitzel, G.; Jackstell, R.; Beller, M. Homogeneous Catalytic Hydrogenation of CO_2 to Methanol − Improvements with Tailored Ligands. *Adv. Synth. Catal.* **2019**, *361* (2), 374−379.

(7) Kanega, R.; Ertem, M. Z.; Onishi, N.; Szalda, D. J.; Fujita, E.; Himeda, Y. CO_2 Hydrogenation and Formic Acid Dehydrogenation Using Ir Catalysts with Amide-Based Ligands. *Organometallics* **2020**, *39* (9), 1519−1531.

(8) Guo, J.; Tian, J.; Deng, J.; Yang, X.; Duan, B.; Liu, Y. Catalytic Reduction of CO_2 by Al−Sn-CNTs Composite for Synthesizing Formic Acid. *Int. J. Hydrogen Energy* **2021**, *46* (58), 29960−29971.

(9) Ren, Y.-Y.; Xia, W.; Deng, B.-Y.; Liu, J.; Wang, F. Host-Guest Assemblies of Anchoring Molecular Catalysts of CO_2 Reduction onto $CuInS_2$/ZnS Quantum Dots for Robust Photocatalytic Syngas Production in Water. *Mol. Catal.* **2022**, *520*, 112168.

(10) Qian, C.; Sun, W.; Hung, D. L. H.; Qiu, C.; Makaremi, M.; Hari Kumar, S. G.; Wan, L.; Ghoussoub, M.; Wood, T. E.; Xia, M.; Tountas, A. A.; Li, Y. F.; Wang, L.; Dong, Y.; Gourevich, I.; Singh, C. V.; Ozin, G. A. Catalytic CO_2 Reduction by Palladium-Decorated Silicon−Hydride Nanosheets. *Nat. Catal.* **2019**, *2* (1), 46−54.

(11) Nam, D.-H.; De Luna, P.; Rosas-Hernández, A.; Thevenon, A.; Li, F.; Agapie, T.; Peters, J. C.; Shekhah, O.; Eddaoudi, M.; Sargent, E. H. Molecular Enhancement of Heterogeneous CO_2 Reduction. *Nat. Mater.* **2020**, *19* (3), 266−276.

(12) Zheng, T.; Jiang, K.; Wang, H. Recent Advances in Electrochemical CO_2-to-CO Conversion on Heterogeneous Catalysts. *Adv. Mater.* **2018**, *30* (48), 1802066.

(13) Rebelein, J. G.; Hu, Y.; Ribbe, M. W. Differential Reduction of CO_2 by Molybdenum and Vanadium Nitrogenases. *Angew. Chem., Int. Ed.* **2014**, *53* (43), 11543−11546.

(14) Jeoung, J.-H.; Dobbek, H. Carbon Dioxide Activation at the Ni,Fe-Cluster of Anaerobic Carbon Monoxide Dehydrogenase. *Science* **2007**, *318* (5855), 1461−1464.

(15) Rebelein, J. G.; Stiebritz, M. T.; Lee, C. C.; Hu, Y. Activation and Reduction of Carbon Dioxide by Nitrogenase Iron Proteins. *Nat. Chem. Biol.* **2017**, *13* (2), 147−149.

(16) Spreitzer, R. J.; Salvucci, M. E. RUBISCO: Structure, Regulatory Interactions, and Possibilities for a Better Enzyme. *Annu. Rev. Plant Biol.* **2002**, *53*, 449−475.

(17) Hügler, M.; Krieger, R. S.; Jahn, M.; Fuchs, G. Characterization of Acetyl-CoA/Propionyl-CoA Carboxylase in Metallosphaera Sedula. *Eur. J. Biochem.* **2003**, *270* (4), 736−744.

(18) Terholsen, H.; Huerta-Zerón, H. D.; Möller, C.; Junge, H.; Beller, M.; Bornscheuer, U. T. Photocatalytic CO_2 Reduction Using CO_2-Binding Enzymes. *Angew. Chem., Int. Ed.* **2024**, *63* (16), e202319313.

(19) Oehlmann, N. N.; Schmidt, F. V.; Herzog, M.; Goldman, A. L.; Rebelein, J. G. The Iron Nitrogenase Reduces Carbon Dioxide to Formate and Methane under Physiological Conditions: A Route to Feedstock Chemicals. *Sci. Adv.* **2024**, *10* (33), eado7729.

(20) Bassegoda, A.; Madden, C.; Wakerley, D. W.; Reisner, E.; Hirst, J. Reversible Interconversion of CO_2 and Formate by a Molybdenum-Containing Formate Dehydrogenase. *J. Am. Chem. Soc.* **2014**, *136* (44), 15473−15476.
(21) Wang, V. C.-C.; Ragsdale, S. W.; Armstrong, F. A. Investigations of Two Bidirectional Carbon Monoxide Dehydrogenases from *Carboxydothermus hydrogenoformans* by Protein Film Electrochemistry. *ChemBioChem* **2013**, *14* (14), 1845−1851.
(22) Bolivar, J. M.; Wilson, L.; Ferrarotti, S. A.; Fernandez-Lafuente, R.; Guisan, J. M.; Mateo, C. Evaluation of Different Immobilization Strategies to Prepare an Industrial Biocatalyst of Formate Dehydrogenase from *Candida boidinii*. *Enzyme Microb. Technol.* **2007**, *40* (4), 540−546.
(23) Jasniewski, A. J.; Lee, C. C.; Ribbe, M. W.; Hu, Y. Reactivity, Mechanism, and Assembly of the Alternative Nitrogenases. *Chem. Rev.* **2020**, *120* (12), 5107−5157.
(24) Einsle, O.; Rees, D. C. Structural Enzymology of Nitrogenase Enzymes. *Chem. Rev.* **2020**, *120* (12), 4969−5004.
(25) Schneider, C. R.; Manesis, A. C.; Stevenson, M. J.; Shafaat, H. S. A Photoactive Semisynthetic Metalloenzyme Exhibits Complete Selectivity for CO_2 Reduction in Water. *Chem. Commun.* **2018**, *54* (37), 4681−4684.
(26) Liu, X.; Kang, F.; Hu, C.; Wang, L.; Xu, Z.; Zheng, D.; Gong, W.; Lu, Y.; Ma, Y.; Wang, J. A Genetically Encoded Photosensitizer Protein Facilitates the Rational Design of a Miniature Photocatalytic CO_2-Reducing Enzyme. *Nat. Chem.* **2018**, *10* (12), 1201−1206.
(27) Alcala-Torano, R.; Halloran, N.; Gwerder, N.; Sommer, D. J.; Ghirlanda, G. Light-Driven CO_2 Reduction by Co-Cytochrome B562. *Front. Mol. Biosci.* **2021**, *8*, 609654.
(28) Deng, Y.; Dwaraknath, S.; Ouyang, W. O.; Matsumoto, C. J.; Ouchida, S.; Lu, Y. Engineering an Oxygen-Binding Protein for Photocatalytic CO_2 Reductions in Water. *Angew. Chem., Int. Ed.* **2023**, *62* (20), e202215719.
(29) Manbeck, G. F.; Fujita, E. A Review of Iron and Cobalt Porphyrins, Phthalocyanines and Related Complexes for Electrochemical and Photochemical Reduction of Carbon Dioxide. *J. Porphyrins Phthalocyanines* **2015**, *19*, 45−64.
(30) Shen, J.; Kortlever, R.; Kas, R.; Birdja, Y. Y.; Diaz-Morales, O.; Kwon, Y.; Ledezma-Yanez, I.; Schouten, K. J. P.; Mul, G.; Koper, M. T. M. Electrocatalytic Reduction of Carbon Dioxide to Carbon Monoxide and Methane at an Immobilized Cobalt Protoporphyrin. *Nat. Commun.* **2015**, *6* (1), 8177.
(31) Call, A.; Cibian, M.; Yamamoto, K.; Nakazono, T.; Yamauchi, K.; Sakai, K. Highly Efficient and Selective Photocatalytic CO_2 Reduction to CO in Water by a Cobalt Porphyrin Molecular Catalyst. *ACS Catal.* **2019**, *9* (6), 4867−4874.
(32) Kalvet, I.; Ortmayer, M.; Zhao, J.; Crawshaw, R.; Ennist, N. M.; Levy, C.; Roy, A.; Green, A. P.; Baker, D. Design of Heme Enzymes with a Tunable Substrate Binding Pocket Adjacent to an Open Metal Coordination Site. *J. Am. Chem. Soc.* **2023**, *145* (26), 14307−14315.
(33) Krishna, R.; Wang, J.; Ahern, W.; Sturmfels, P.; Venkatesh, P.; Kalvet, I.; Lee, G. R.; Morey-Burrows, F. S.; Anishchenko, I.; Humphreys, I. R.; McHugh, R.; Vafeados, D.; Li, X.; Sutherland, G. A.; Hitchcock, A.; Hunter, C. N.; Kang, A.; Brackenbrough, E.; Bera, A. K.; Baek, M.; DiMaio, F.; Baker, D. Generalized Biomolecular Modeling and Design with RoseTTAFold All-Atom. *Science* **2024**, *384* (6693), eadl2528.
(34) Dauparas, J.; Lee, G. R.; Pecoraro, R.; An, L.; Anishchenko, I.; Glasscock, C.; Baker, D. Atomic Context-Conditioned Protein Sequence Design Using LigandMPNN Nature Methods. *Nat. Methods.* **2025**, *22* (4), 717−723.
(35) Perkins, L. J.; Weaver, B. R.; Buller, A. R.; Burstyn, J. N. De Novo Biosynthesis of a Nonnatural Cobalt Porphyrin Cofactor in *E. coli* and Incorporation into Hemoproteins. *Proc. Natl. Acad. Sci. U. S. A.* **2021**, *118* (16), e2017625118.
(36) Teale, F. W. J. Cleavage of the Haem-Protein Link by Acid Methylethylketone. *Biochim. Biophys. Acta* **1959**, *35*, 543.
(37) Kawakami, N.; Shoji, O.; Watanabe, Y. Single-Step Reconstitution of Apo-Hemoproteins at the Disruption Stage of *Escherichia coli* Cells. *ChemBioChem* **2012**, *13* (14), 2045−2047.
(38) Sumida, K. H.; Núñez-Franco, R.; Kalvet, I.; Pellock, S. J.; Wicky, B. I. M.; Milles, L. F.; Dauparas, J.; Wang, J.; Kipnis, Y.; Jameson, N.; Kang, A.; De La Cruz, J.; Sankaran, B.; Bera, A. K.; Jiménez-Osés, G.; Baker, D. Improving Protein Expression, Stability, and Function with ProteinMPNN. *J. Am. Chem. Soc.* **2024**, *146* (3), 2054−2061.
(39) Kim, D. E.; Watson, J. L.; Juergens, D.; Majumder, S.; Sonigra, R.; Gerben, S. R.; Kang, A.; Bera, A. K.; Li, X.; Baker, D. Parametrically Guided Design of Beta Barrels and Transmembrane Nanopores Using Deep Learning. *Proc. Natl. Acad. Sci. U. S. A.* **2025**, *122* (38), e2425459122.
(40) Lee, G. R.; Pellock, S. J.; Norn, C.; Tischer, D.; Dauparas, J.; Anishchenko, I.; Mercer, J. A. M.; Kang, A.; Bera, A. K.; Nguyen, H.; Brackenbrough, E.; Sankaran, B.; Goreshnik, I.; Vafeados, D.; Roullier, N.; Han, H. L.; Coventry, B.; Haddox, H. K.; Liu, D. R.; Yeh, A. H.-W.; Baker, D. Small-Molecule Binding and Sensing with a Designed Protein Family. *Nat. Commun.* **2026**, *17*, 4533.
(41) Basanta, B.; Bick, M. J.; Bera, A. K.; Norn, C.; Chow, C. M.; Carter, L. P.; Goreshnik, I.; Dimaio, F.; Baker, D. An Enumerative Algorithm for De Novo Design of Proteins with Diverse Pocket Structures. *Proc. Natl. Acad. Sci. U. S. A.* **2020**, *117* (36), 22135−22145.
(42) Marcos, E.; Basanta, B.; Chidyausiku, T. M.; Tang, Y.; Oberdorfer, G.; Liu, G.; Swapna, G. V. T.; Guan, R.; Silva, D.-A.; Dou, J.; Pereira, J. H.; Xiao, R.; Sankaran, B.; Zwart, P. H.; Montelione, G. T.; Baker, D. Principles for Designing Proteins with Cavities Formed by Curved β Sheets. *Science* **2017**, *355* (6321), 201−206.
(43) Dauparas, J.; Anishchenko, I.; Bennett, N.; Bai, H.; Ragotte, R. J.; Milles, L. F.; Wicky, B. I. M.; Courbet, A.; de Haas, R. J.; Bethel, N.; Leung, P. J. Y.; Huddy, T. F.; Pellock, S.; Tischer, D.; Chan, F.; Koepnick, B.; Nguyen, H.; Kang, A.; Sankaran, B.; Bera, A. K.; King, N. P.; Baker, D. Robust Deep Learning−Based Protein Sequence Design Using ProteinMPNN. *Science* **2022**, *378* (6615), 49−56.
(44) Tyka, M. D.; Keedy, D. A.; André, I.; DiMaio, F.; Song, Y.; Richardson, D. C.; Richardson, J. S.; Baker, D. Alternate States of Proteins Revealed by Detailed Energy Landscape Mapping. *J. Mol. Biol.* **2011**, *405* (2), 607−618.
(45) Jumper, J.; Evans, R.; Pritzel, A.; Green, T.; Figurnov, M.; Ronneberger, O.; Tunyasuvunakool, K.; Bates, R.; Žídek, A.; Potapenko, A.; Bridgland, A.; Meyer, C.; Kohl, S. A. A.; Ballard, A. J.; Cowie, A.; Romera-Paredes, B.; Nikolov, S.; Jain, R.; Adler, J.; Back, T.; Petersen, S.; Reiman, D.; Clancy, E.; Zielinski, M.; Steinegger, M.; Pacholska, M.; Berghammer, T.; Bodenstein, S.; Silver, D.; Vinyals, O.; Senior, A. W.; Kavukcuoglu, K.; Kohli, P.; Hassabis, D. Highly Accurate Protein Structure Prediction with AlphaFold. *Nature* **2021**, *596* (7873), 583−589.
(46) Wicky, B. I. M.; Milles, L. F.; Courbet, A.; Ragotte, R. J.; Dauparas, J.; Kinfu, E.; Tipps, S.; Kibler, R. D.; Baek, M.; DiMaio, F.; Li, X.; Carter, L.; Kang, A.; Nguyen, H.; Bera, A. K.; Baker, D. Hallucinating Symmetric Protein Assemblies. *Science* **2022**, *378* (6615), 56−61.
(47) Qian, J.; Milles, L. F.; Wicky, B. I. M.; Ragotte, R. J.; Motmaen, A.; Borst, A. J.; Skotheim, R.; Ols, S.; Coventry, B.; Li, X.; Kibler, R. D.; Goreshnik, I.; Expòsit, M.; Loré, K.; Stewart, L.; Baker, D. Accelerating Protein Design by Scaling Experimental Characterization. *bioRxiv* **2025**, DOI: 10.1101/2025.08.05.668824.
(48) Labidi, R. J.; Faivre, B.; Carpentier, P.; Perard, J.; Gotico, P.; Li, Y.; Atta, M.; Fontecave, M. Light-Activated Artificial CO_2-Reductase: Structure and Activity. *J. Am. Chem. Soc.* **2024**, *146* (41), 28296−28305.
(49) Sommer, D. J.; Vaughn, M. D.; Ghirlanda, G. Protein Secondary-Shell Interactions Enhance the Photoinduced Hydrogen Production of Cobalt Protoporphyrin IX. *Chem. Commun.* **2014**, *50* (100), 15852−15855.

(50) Yadav, R.; Scott, E. E. Endogenous Insertion of Non-Native Metalloporphyrins into Human Membrane Cytochrome P450 Enzymes. *J. Biol. Chem.* **2018**, *293* (43), 16623−16634.
(51) Sakurai, H.; Ishizu, K.; Sugimoto, H.; Gunsalus, I. C. Model of the Coordination Site for Cobalt-Substituted Cytochrome P450cam. *J. Inorg. Biochem.* **1986**, *26* (1), 55−62.
(52) Zhang, Y.; Skolnick, J. TM-Align: A Protein Structure Alignment Algorithm Based on the TM-Score. *Nucleic Acids Res.* **2005**, *33* (7), 2302−2309.
(53) Hawecker, J.; Lehn, J.-M.; Ziessel, R. Photochemical Reduction of Carbon Dioxide to Formate Mediated by Ruthenium Bipyridine Complexes as Homogeneous Catalysts. *J. Chem. Soc., Chem. Commun.* **1985**, No. 2, 56−58.
(54) Abramson, J.; Adler, J.; Dunger, J.; Evans, R.; Green, T.; Pritzel, A.; Ronneberger, O.; Willmore, L.; Ballard, A. J.; Bambrick, J.; Bodenstein, S. W.; Evans, D. A.; Hung, C.-C.; O'Neill, M.; Reiman, D.; Tunyasuvunakool, K.; Wu, Z.; Žemgulytė, A.; Arvaniti, E.; Beattie, C.; Bertolli, O.; Bridgland, A.; Cherepanov, A.; Congreve, M.; Cowen-Rivers, A. I.; Cowie, A.; Figurnov, M.; Fuchs, F. B.; Gladman, H.; Jain, R.; Khan, Y. A.; Low, C. M. R.; Perlin, K.; Potapenko, A.; Savy, P.; Singh, S.; Stecula, A.; Thillaisundaram, A.; Tong, C.; Yakneen, S.; Zhong, E. D.; Zielinski, M.; Žídek, A.; Bapst, V.; Kohli, P.; Jaderberg, M.; Hassabis, D.; Jumper, J. M. Accurate Structure Prediction of Biomolecular Interactions with AlphaFold 3. *Nature* **2024**, *630* (8016), 493−500.
(55) Radley, E.; Andrews, A.; Kalvet, I.; Deng, Y.; Levy, C. W.; Ortmayer, M.; Heyes, D. J.; Megarity, C. F.; Núñez-Franco, R.; Hutton, A. E.; Lu, Y.; Baker, D.; Green, A. P. A De Novo CO_2 Reductase Featuring a Cysteine-Ligated Cobalt Porphyrin Cofactor. *Zenodo* **2026**, DOI: 10.5281/zenodo.1861569955.

https://doi.org/10.1021/jacs.6c07615
J. Am. Chem. Soc. XXXX, XXX, XXX−XXX